The Journal of Chemical Physics

A full-dimensional quantum approach to the vibrational predissociation of tetra-atomic complexes based on the partially-separable time-dependent self-consistent-field approximation

Cite as: J. Chem. Phys. **116**, 6595 (2002); https://doi.org/10.1063/1.1461823
Submitted: 24 September 2001 . Accepted: 24 January 2002 . Published Online: 02 April 2002

A. García-Vela

A full-dimensional quantum approach to the vibrational predissociation of tetra-atomic complexes based on the partially-separable time-dependent self-consistent-field approximation

A. García-Vela[a)]
Instituto de Matemáticas y Física Fundamental, C.S.I.C., Serrano 123, 28006 Madrid, Spain

(Received 24 September 2001; accepted 24 January 2002)

A full-dimensional time-dependent quantum approach is proposed to study the vibrational predissociation (VP) dynamics of $BC-Rg_2$ (BC=diatomic molecule, Rg=rare-gas atom) clusters. The method applies the partially-separable time-dependent self-consistent-field approximation to express the six-dimensional total wave function as a product of two wave functions, one describing the three stretching modes of the system, the other one describing the three bending modes. The method is tested by simulating the VP of Cl_2-Ne_2 for the initial Cl_2 vibrational excitations $v=7-13$, and of $I_2(v=21)-Ne_2$. The Cl_2-Ne_2 results are compared to experimental data and earlier simulations. The method is very efficient as compared to previous reduced-dimensional quantum models where the bending modes were not explicitly considered in the dynamics. Good agreement with experiment is found for the resonance lifetimes and Cl_2 vibrational distributions for $v\geqslant 9$, where the bending/stretching couplings are not strong. The model underestimates rotational excitation of the Cl_2 fragment, failing to reproduce the Cl_2 rotational distributions. In the case of I_2 $(v=21)-Ne_2$, the time evolution of the vibrational populations is compared with previous multiconfiguration time-dependent Hartree calculations. The favorable comparison obtained supports the reliability of the method within certain validity conditions. © *2002 American Institute of Physics.* [DOI: 10.1063/1.1461823]

I. INTRODUCTION

Weakly bound van der Waals (vdW) clusters $BC-Rg_n$ (BC=diatomic molecule, Rg=rare gas atom) are prototype systems to explore fundamental aspects of energy transfer processes which take place upon excitation of the diatomic subunit. Such processes include vibrational predissociation, intramolecular vibrational redistribution (IVR), and evaporative cooling. In the last two decades a variety of vdW clusters has been investigated using both frequency-domain and time-domain techniques. Among the frequency-domain experiments are predissociation dynamics studies of I_2-He_n $(n=1-3)$,[1] I_2-Ne_n $(n=1-7)$,[2,3] Br_2-Ne_n $(n=1-3)$,[4] $ICl-Ne_n$ $(n=1-5)$,[5] Cl_2-Ne_n $(n=1-3)$,[6] Cl_2-Ar_n $(n=1-3)$,[7] and Cl_2-He_n $(n=1,2)$.[8] Time-domain techniques have been applied to investigate the VP dynamics of I_2-Ne_n $(n=1-4)$.[9]

From the theoretical point of view, the predissociation dynamics of several vdW clusters has also been studied. Most exact quantum dynamics calculations have been limited to triatomic BC–Rg complexes.[10–14] The VP dynamics of larger clusters like I_2-He_n $(n=1-9)$,[15] I_2-Ne_n $(n=1-9)$,[16,17] and I_2-Ar_{13},[18] was investigated by means of classical and quasiclassical simulations. Full-dimensional hybrid classical-quantum and quantum-classical approaches were applied to study the predissociation dynamics of Cl_2-He_2,[19] I_2-Ne_n $(n=2-6)$,[20] and Cl_2-Ne_n $(n=2,3)$.[21] Quantum dynamical calculations on tetraatomic $BC-Rg_2$ complexes have been reported using reduced-dimensional models including three coupled degrees of freedom[22–25] (in Ref. 24 a fourth degree of freedom was also considered in the framework of the time-dependent Hartree approximation), and four coupled degrees of freedom.[26] Full-dimensional quantum calculations on the VP of I_2-Ne_2 have been recently reported using the multiconfiguration time-dependent Hartree (MCTDH) method.[27] Application of the MCTDH formalism to $BC-Rg_2$ systems is promising although it is still very demanding.

In general, the full-dimensional classical and hybrid methods and the reduced-dimensional quantum (RDQ) models are able to predict the main dynamical features observed experimentally. However, a quantitative level of prediction of all the experimental data is not yet achieved by these treatments. Leaving aside the quality of the potential surfaces employed, the classical and hybrid approaches lack quantum effects, while the RDQ models lack the influence of the modes neglected. One possible direction to improve the quantum description is to add one more fully-coupled degree of freedom to the presently available RDQ models. Typically this involves much computational effort, and it is not clear *a priori* that the improvement of the description is worth such an effort. Another approach, computationally affordable, is to consider the full dimensionality of the system and to apply a scheme of separation of some of the modes, in order to make the quantum mechanical problem tractable. This latter approach has been adopted in this work.

In the present paper a full-dimensional quantum dynamical treatment of the VP of $BC-Rg_2$ systems is proposed. The

a)Electronic mail: garciavela@imaff.cfmac.csic.es

TABLE I. Calculated full-dimensional (this work) and reduced-dimensional (Ref. 23) resonance energies relative to the initial Cl_2 vibrational energy level E_v. $E_v=0$ corresponds to separated atoms.

	$v=7$	$v=8$	$v=9$	$v=10$	$v=11$	$v=12$	$v=13$
$E_v(cm^{-1})$	−1511.1	−1338.0	−1175.4	−1023.3	−881.8	−750.8	−630.3
$E_{res}(cm^{-1})$[a]	−125.67	−125.43	−125.24	−124.86	−124.59	−124.19	−123.67
$E_{res}(cm^{-1})$[b]	−152.3	−152.13	−151.97	−151.26	−151.48	−151.15	−150.67

[a]This work.
[b]Reference 23.

method suggested applies the partially-separable time-dependent self-consistent-field (PS TDSCF) approximation[28] to divide the system modes into two groups, where the modes within each group remain fully coupled during the dynamics. Specifically, the total six-dimensional wave function of the system is expressed as a product of two wave functions, one of them describing the three stretching modes of the complex, and the other one describing the three bending modes. Upon time propagation, the TDSCF equations allow the two partial wave functions to interact during the dynamics, through mean-field, effective Hamiltonians. At any time each group of modes feels the average dynamical influence of the other modes. The approach is tested by simulating the VP dynamics of Cl_2-Ne_2, a system for which there are available experimental data[6] and different theoretical studies[21,23,25] to compare with. An additional test of the method is carried out by simulating the VP of I_2-Ne_2 and comparing the results with the recent MCTDH calculations.[27]

The outline of the paper is the following: In Sec. II the VP process and the system are briefly described, and the approach suggested is presented. Results are compared with those of experiment and previous theoretical studies, and discussed in Sec. III. Some conclusions are drawn in Sec. IV.

II. THE APPROACH

A. The process and the system

Upon excitation of the Cl_2 chromophore in Cl_2-Ne_2 from the ground electronic state to a vibrational state $v>0$ in the excited B electronic state, a resonance state $Cl_2^*(B,v)-Ne_2$ is prepared. From that state the complex undergoes vibrational predissociation, decaying to a fragmentation continuum. Energy transfer from the Cl_2 stretching vibration to the vdW modes is what causes fragmentation of the complex, which can follow different pathways,

$$Cl_2^*(B,v)-Ne_2 \rightarrow Cl_2(B,v'<v)-Ne+Ne \rightarrow Cl_2(B,v''<v')+Ne+Ne, \quad (1)$$

$$Cl_2^*(B,v)-Ne_2 \rightarrow Cl_2(B,v'<v)+Ne+Ne, \quad (2)$$

$$Cl_2^*(B,v)-Ne_2 \rightarrow Cl_2(B,v'<v)+Ne_2. \quad (3)$$

The VP process can be assumed, to a good approximation, to occur on a single potential-energy surface, that of the B electronic state. Similarly as in previous theoretical studies, this potential surface is modeled as a sum of pairwise atom–atom interactions, each of them described by a Morse function. The Morse parameters used in the calculations are the same as those employed in earlier simulations.[21,23,25]

B. Representation of the system and initial state

The Cl_2-Ne_2 system is represented in bond coordinates $(\mathbf{r},\mathbf{R_1},\mathbf{R_2})$, where $\mathbf{r}$ is the vector associated with the Cl–Cl bond distance, and $\mathbf{R_1}$, $\mathbf{R_2}$ are the vectors between the Cl_2 center-of-mass and the two Ne atoms, respectively. By expressing the vectors $\mathbf{r}$, $\mathbf{R_1}$, and $\mathbf{R_2}$ in spherical coordinates $[\mathbf{r}=(r,\theta_r,\phi_r),\mathbf{R_i}=(R_i,\theta_i,\phi_i),i=1,2]$ the Hamiltonian of the system can be written as

$$\hat{H}=-\frac{\hbar^2}{2\mu_{Cl_2}}\frac{\partial^2}{\partial r^2}+\frac{\mathbf{j}^2}{2\mu_{Cl_2}r^2}-\frac{\hbar^2}{2\mu_{Cl_2-Ne}}\left(\frac{\partial^2}{\partial R_1^2}+\frac{\partial^2}{\partial R_2^2}\right)+\frac{1}{2\mu_{Cl_2-Ne}}\left(\frac{\mathbf{l_1}^2}{R_1^2}+\frac{\mathbf{l_2}^2}{R_2^2}\right)-\frac{\hbar^2\boldsymbol{\nabla}_1\cdot\boldsymbol{\nabla}_2}{2m_{Cl}}+V(\mathbf{r},\mathbf{R_1},\mathbf{R_2}), \quad (4)$$

where $\mu_{Cl_2}=m_{Cl}/2$ and $\mu_{Cl_2-Ne}=m_{Ne}2m_{Cl}/(m_{Ne}+2m_{Cl})$ are the reduced masses corresponding to the Cl_2 and vdW modes, respectively, and $\mathbf{j}$, $\mathbf{l_1}$, and $\mathbf{l_2}$ are the angular momentum operators associated with $\mathbf{r}$, $\mathbf{R_1}$, and $\mathbf{R_2}$, respectively (the total angular momentum of the system is $\mathbf{J}=\mathbf{j}+\mathbf{l_1}+\mathbf{l_2}$). An expanded expression of $\boldsymbol{\nabla}_1\cdot\boldsymbol{\nabla}_2$ is given in Ref. 25.

Before carrying out the simulation of the VP dynamics, the initial state of Cl_2-Ne_2 prepared by excitation needs to be specified. Such initial state corresponds with the ground resonance state of the complex (assuming that $J=0$) associated to the specific Cl_2 vibrational level v excited in the B electronic state. In order to calculate this initial state the variational formalism of Villarreal *et al.*[29] has been applied. To this purpose the Hamiltonian of Eq. (4) is represented in a suitable basis set and diagonalized. Details on these calculations have been given elsewhere.[25]

Calculated resonance energies are listed in Table I for the different vibrational states v of Cl_2 studied ($v=7-13$), and compared with the energies obtained with the RDQ model of Ref. 23. It should be noted that due to a typographical mistake, in Table II of Ref. 25 the resonance energy for $v=11$ reads $-123.97\ cm^{-1}$, instead of the correct value $-124.59\ cm^{-1}$ included in the present Table I. The vibrational energies of Cl_2, E_v are also given in Table I. The present energies E_v are about $10\ cm^{-1}$ lower than those of Ref. 23, probably due to a slightly different chlorine mass used here ($m_{Cl}=35.4527$ amu).

C. The PS TDSCF equations

In the present approach a partially-separable ansatz is assumed for the exact total wave function $\Psi(r,R_1,R_2,\theta_1,\theta_2,\phi,t)$ of the system, which is approximated by $\Psi^{\mathrm{TDSCF}}(r,R_1,R_2,\theta_1,\theta_2,\phi,t)$,

$$\Psi^{\mathrm{TDSCF}}(r,R_1,R_2,\theta_1,\theta_2,\phi,t) = \psi(r,R_1,R_2,t)\Phi(\theta_1,\theta_2,\phi,t)e^{\imath\gamma(t)}, \quad (5)$$

where the phase factor $e^{\imath\gamma(t)}$ is a coordinate-independent factor[30,31] which arises as a consequence of factorizing $\Psi(r,R_1,R_2,\theta_1,\theta_2,\phi,t)$, and ϕ is defined as $\phi=\phi_1-\phi_2$. By introducing the ansatz of Eq. (5) into the Schrödinger equation,

$$\imath\hbar\frac{\partial\Psi(r,R_1,R_2,\theta_1,\theta_2,\phi,t)}{\partial t} = \hat{H}\Psi(r,R_1,R_2,\theta_1,\theta_2,\phi,t), \quad (6)$$

three new equations of motion are found for $\psi(r,R_1,R_2,t)$, $\Phi(\theta_1,\theta_2,\phi,t)$, and $\gamma(t)$,

$$\imath\hbar\frac{\partial\psi(r,R_1,R_2,t)}{\partial t} = \hat{H}_1^{\mathrm{eff}}(r,R_1,R_2,t)\psi(r,R_1,R_2,t), \quad (7)$$

$$\imath\hbar\frac{\partial\Phi(\theta_1,\theta_2,\phi,t)}{\partial t} = \hat{H}_2^{\mathrm{eff}}(\theta_1,\theta_2,\phi,t)\Phi(\theta_1,\theta_2,\phi,t), \quad (8)$$

$$\gamma(t) = \int_0^t dt'\hat{H}_3^{\mathrm{eff}}(t'), \quad (9)$$

where $\hat{H}_1^{\mathrm{eff}}(r,R_1,R_2,t)$, $\hat{H}_2^{\mathrm{eff}}(\theta_1,\theta_2,\phi,t)$, and $\hat{H}_3^{\mathrm{eff}}(t')$ are time-dependent effective mean-field Hamiltonians defined as

$$\hat{H}_1^{\mathrm{eff}}(r,R_1,R_2,t) = \langle\Phi(\theta_1,\theta_2,\phi,t)|\hat{H}|\Phi(\theta_1,\theta_2,\phi,t)\rangle, \quad (10)$$

$$\hat{H}_2^{\mathrm{eff}}(\theta_1,\theta_2,\phi,t) = \langle\psi(r,R_1,R_2,t)|\hat{H}|\psi(r,R_1,R_2,t)\rangle, \quad (11)$$

$$\hat{H}_3^{\mathrm{eff}}(t) = \langle\psi(r,R_1,R_2,t)\Phi(\theta_1,\theta_2,\phi,t) \times|\hat{H}|\psi(r,R_1,R_2,t)\Phi(\theta_1,\theta_2,\phi,t)\rangle. \quad (12)$$

The PS TDSCF equations, Eqs. (7)–(12) are solved self-consistently, and the effective Hamiltonians allow for partial interaction between $\psi(r,R_1,R_2,t)$ and $\Phi(\theta_1,\theta_2,\phi,t)$ during the dynamical evolution.

In order to solve Eq. (7) the wave packet $\psi(r,R_1,R_2,t)$ is expanded on the vibrational eigenstates $\chi_\nu(r)$ of Cl_2 as

$$\psi(r,R_1,R_2,t) = \sum_\nu C_\nu(R_1,R_2,t)\chi_\nu(r)e^{-iE_\nu t/\hbar}, \quad (13)$$

where $\chi_\nu(r)$ is obtained as a numerical solution of

$$\left[-\frac{\hbar^2}{2\mu_{\mathrm{Cl}_2}}\frac{\partial^2}{\partial r^2}+V_{\mathrm{Cl}_2}(r)\right]\chi_\nu(r) = E_\nu\chi_\nu(r). \quad (14)$$

Introducing the expansion of Eq. (13) in Eq. (7) leads to a set of time-dependent coupled equations for the different $C_\nu(R_1,R_2,t)$ packets, which are the equations actually solved. Four terms in the expansion of Eq. (13), $\nu=v,v-1,v-2$, and $v-3$ are sufficient to describe the VP dynamics of Cl_2-Ne_2.

A general packet $\Phi_\Omega^{J,M}(\theta_1,\theta_2,\phi_1,\phi_2,t)$ can be expanded on an angular basis set,

$$\Phi_\Omega^{J,M}(\theta_1,\theta_2,\phi_1,\phi_2,t) = \sum_{l_1,l_2,L} c_{l_1,l_2,L,\Omega}^{J,M}(t)\,\eta_{l_1,l_2,L,\Omega}^{J,M} \times(\theta_1,\theta_2,\phi_1,\phi_2), \quad (15)$$

where $L=l_1+l_2$, and M and Ω are the projections of J on the Z axes of the space-fixed (SF) and body-fixed (BF) frames, respectively (the Z_{BF} axis coincides with the direction of the **r** vector). The angular basis functions are defined as

$$\eta_{l_1,l_2,L,\Omega}^{J,M}(\theta_1,\theta_2,\phi_1,\phi_2) = \left[\frac{1}{2(1+\delta_{l_1l_2})}\right]^{1/2} \times[\mathcal{W}_{l_1,l_2,L,\Omega}^{J,M}(\theta_1,\theta_2,\phi_1,\phi_2) + \mathcal{W}_{l_2,l_1,L,\Omega}^{J,M}(\theta_1,\theta_2,\phi_1,\phi_2)], \quad (16)$$

The definition of Eq. (16) takes into account the angular symmetry of the Cl_2-Ne_2 Hamiltonian, i.e., the Hamiltonian is invariant under exchange of $\mathbf{l_1}$ and $\mathbf{l_2}$. The functions $\mathcal{W}_{l_1,l_2,L,\Omega}^{J,M}(\theta_1,\theta_2,\phi_1,\phi_2)$ are defined as

$$\mathcal{W}_{l_1,l_2,L,\Omega}^{J,M}(\theta_1,\theta_2,\phi_1,\phi_2) = \left(\frac{2J+1}{4\pi}\right)^{1/2} D_{M,\Omega}^{J*}(\phi_r,\theta_r,0) \times\mathcal{Y}_{l_1,l_2}^{L,\Omega}(\theta_1,\theta_2,\phi_1,\phi_2), \quad (17)$$

where $D_{M,\Omega}^{J*}$ are Wigner rotation matrices[32,33] which relate the SF and BF frames. The functions $\mathcal{Y}_{l_1,l_2}^{L,\Omega}(\theta_1,\theta_2,\phi_1,\phi_2)$ are expressed as

$$\mathcal{Y}_{l_1,l_2}^{L,\Omega}(\theta_1,\theta_2,\phi_1,\phi_2) = (-1)^{L+\Omega}(2L+1)^{1/2} \times\sum_\omega \begin{pmatrix} l_1 & l_2 & L \\ -\omega & \omega-\Omega & \omega \end{pmatrix} \times Y_{l_1}^{\omega}(\theta_1,\phi_1)Y_{l_2}^{\Omega-\omega}(\theta_2,\phi_2), \quad (18)$$

where $(\cdots)$ denotes $3-j$ symbols and $Y_{l_i}^{\omega}(\theta_i,\phi_i)$ are spherical harmonics. In the present dynamical treatment $J=0$ is assumed, which implies that $M=\Omega=0$, and $\mathbf{L}=-\mathbf{j}$. When $J=0$ the two angular coordinates ϕ_1 and ϕ_2 are not independent, and they can be grouped into a single, independent one, $\phi=\phi_1-\phi_2$. Thus the general angular wave packet $\Phi_\Omega^{J,M}(\theta_1,\theta_2,\phi_1,\phi_2,t)$ becomes $\Phi_0^{0,0}(\theta_1,\theta_2,\phi,t)$. For the sake of compactness the indices J, M, and Ω have been omitted when referring to $\Phi(\theta_1,\theta_2,\phi,t)$ in Sec. II C, and the same criterion will be kept hereafter. The expression of Eq. (15) can be simplified to a more compact form,

$$\Phi(\theta_1,\theta_2,\phi,t)=\sum_{l_1,l_2,L} c_{l_1,l_2,L}(t)\,\eta_{l_1,l_2,L}(\theta_1,\theta_2,\phi), \tag{19}$$

where $c_{l_1,l_2,L}(t)=c^{0,0}_{l_1,l_2,L,0}(t)$ and $\eta_{l_1,l_2,L}(\theta_1,\theta_2,\phi)=\eta^{0,0}_{l_1,l_2,L,0}(\theta_1,\theta_2,\phi_1,\phi_2)$. By representing the Hamiltonian $\hat{H}_2^{\rm eff}(\theta_1,\theta_2,\phi,t)$ in the basis set of the functions $\eta_{l_1,l_2,L}(\theta_1,\theta_2,\phi)$, Eq. (8) is transformed into a set of time-dependent coupled equations for the coefficients $c_{l_1,l_2,L}(t)$. Solution of this set of coupled equations provides the time evolution of the angular wave packet $\Phi(\theta_1,\theta_2,\phi,t)$.

By expanding the angular dependence of the $V(\mathbf{r},\mathbf{R_1},\mathbf{R_2})$ interaction potential on spherical harmonics, the angular quadratures of the potential terms of $\hat{H}$ and $\hat{H}_2^{\rm eff}(\theta_1,\theta_2,\phi,t)$ over the basis functions $\eta_{l_1,l_2,L}(\theta_1,\theta_2,\phi)$ become analytical.[29] All the remaining quadratures over the angular basis functions of angular operators of $\hat{H}$ and $\hat{H}_2^{\rm eff}(\theta_1,\theta_2,\phi,t)$ ($\mathbf{j}^2$, $\mathbf{l_1}^2$, $\mathbf{l_2}^2$, and the angular dependence of $\mathbf{\nabla_1}\cdot\mathbf{\nabla_2}$) can also be evaluated analytically.[29] This makes very efficient the representation of $\hat{H}$ and $\hat{H}_2^{\rm eff}(\theta_1,\theta_2,\phi,t)$ in the basis set $\eta_{l_1,l_2,L}(\theta_1,\theta_2,\phi)$, and the calculation of the time-dependent effective Hamiltonians of Eqs. (10)–(12).

Some comments on the PS TDSCF approach presented above are now due. The energy initially deposited in the BC vibration can flow freely towards the reactive coordinates R_1 and R_2, since the exact, full couplings between the three stretching modes are retained in the model. By contrast, the explicit breaking of the couplings between the stretching and the bending modes assumed in Eq. (5), precludes the possibility of an exact interaction and energy flow between r (and R_1,R_2) and the bending modes. In the approach such couplings are recovered only partially through the time-dependent effective Hamiltonians. Therefore, this model is expected to underestimate energy transfer to the rotational modes. In the present treatment the bending modes are considered as bath modes which are coupled dynamically, albeit approximately, to the reactive stretching modes.

Recently, a RDQ model for the VP dynamics of BC–Rg_2 systems which incorporates in a systematic way the full-dimensional energy of the system was suggested.[25] This model was applied to Cl_2–Ne_2 and considered three coupled degrees of freedom, namely, the three stretching modes of the system. In essence, in the model of Ref. 25 a similar separation of the total wave function as that of Eq. (5) was assumed, and an equation like Eq. (7) was solved, where the effective Hamiltonian was not time-dependent, but defined as

$$\hat{H}^{\rm eff}(r,R_1,R_2)=\langle\Phi(\theta_1,\theta_2,\phi,t=0)|\hat{H}|\Phi(\theta_1,\theta_2,\phi,t=0)\rangle. \tag{20}$$

The approach proposed here can be viewed as a generalization of the RDQ model of Ref. 25 by incorporating the average dynamical effect of the bending modes at any time t. In this sense, in the present method, same as in the model of Ref. 25, the predissociation dynamics takes place at the full-dimensional energy of the system.

D. Computational details

The $C_\nu(R_1,R_2,t)$ packets are represented on a uniform grid in the R_1 and R_2 coordinates. The grid parameters are $R_0=4.0$ a.u., $\Delta R=0.25$ a.u., and the number of grid points $N_R=256$. All the Hamiltonian operations on $C_\nu(R_1,R_2,t)$ involving kinetic-energy terms are performed using fast Fourier transform (FFT) techniques. The angular wave packet $\Phi(\theta_1,\theta_2,\phi_1,t)$ is expanded on 660 angular basis functions $\eta_{l_1,l_2,L}(\theta_1,\theta_2,\phi)$, with $l_1^{\max}=l_2^{\max}=20$ and $L^{\max}=18$. The time propagation of the $C_\nu(R_1,R_2,t)$ packets and the $c_{l_1,l_2,L}(t)$ coefficients was carried out by means of the Chebychev polynomial expansion method,[34] with time steps $\Delta t_1=0.01$ ps and $\Delta t_2=0.000\,625$ ps, respectively.

The $\psi(r,R_1,R_2,t)$ wave packet is absorbed before it reaches the edges of the grid in the R_1 and R_2 coordinates. Absorption is carried out after each time step Δt_1 by multiplying each packet $C_\nu(R_1,R_2,t)$ by a product of exponential functions in R_1 and R_2, as described elsewhere.[23,25] The parameters used for the absorption exponential functions are $\alpha=0.20$ a.u.$^{-2}$ and $R_{\rm abs}=57.0$ a.u. For the analysis of product distributions the vdW bonds are considered effectively broken for distances $R_1,R_2>R_c=15$ a.u.

The absorption of $\psi(r,R_1,R_2,t)$ causes its norm to decrease with time, and this can affect the calculation of the effective Hamiltonians $\hat{H}_2^{\rm eff}(\theta_1,\theta_2,\phi,t)$ and $\hat{H}_3^{\rm eff}(t)$ of Eqs. (11) and (12). In order to minimize such an effect, the strategy adopted here has been to increase the grid size and to place the beginning of the absorption region farther away in the asymptotic region. In previous RDQ calculations[23,25] the grid size used was $N_R=128$ with $R_{\rm abs}=25.0$ a.u., while here $N_R=256$ and $R_{\rm abs}=57.0$ a.u. With the present grid and absorption parameters the minimization effect obtained is twofold. First, the accumulated amount of $\psi(r,R_1,R_2,t)$ absorbed during the whole time propagation is $<5\%$ for the calculations carried out for the different initial resonance states (and typically $<3\%$). Second, this small portion of the wave packet is absorbed in the far asymptotic region where many terms of the Hamiltonian $\hat{H}$ which are averaged over $\psi(r,R_1,R_2,t)$ in Eqs. (11) and (12) have vanished or nearly vanished. Therefore, the effect of the absorption on the calculation of the effective Hamiltonians can be considered negligible.

III. RESULTS AND DISCUSSION

A. Resonance lifetimes

The decay of the resonance states of Cl_2–Ne_2 associated with the vibrational levels $v=7-13$ of Cl_2 has been simulated. The wave packet propagation was carried out until different final times t_f, depending on the vibrational state excited. Specifically, $t_f=15$ ps for $v=7,8,9$, $t_f=13$ ps for $v=10,11$, and $t_f=10$ ps for $v=12,13$. The resonance decay curves are calculated as the square of the total wave packet autocorrelation function $P(t)=|C(t)|^2=|\langle\Psi^{\rm TDSCF}(0)|\times\Psi^{\rm TDSCF}(t)\rangle|^2$. It has been shown[35] that by propagating the wave packet until a final time t_f, one can obtain $C(t)$ [and therefore $P(t)$] until a time $2t_f$. Thus $|C(t)|^2$ has been cal-

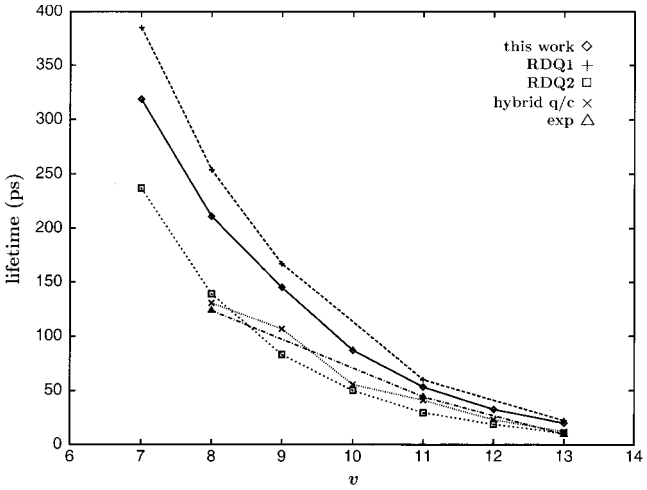

FIG. 1. Plot of the calculated and experimental resonance lifetimes presented in Table II vs the initial Cl_2 vibrational level v.

culated until $t=2t_f$, following the procedure described in Ref. 25 to take into account that the wave packet is absorbed during the time propagation.

Resonance lifetimes can be extracted from the calculated decay curves by fitting them to an exponential law,

$$P(t)\simeq e^{-(t/\tau)}. \tag{21}$$

Exponential fits to the calculated decay curves similar to those shown in Fig. 1 of Ref. 25 are obtained. The resonance decay lifetimes found are listed in Table II along with the experimental lifetimes and those previously calculated. For the sake of comparison all the lifetimes are plotted in Fig. 1 versus the initial vibrational quantum number v.

The present lifetimes improve significantly over the lifetimes obtained with the RDQ model of Ref. 25, as a consequence of including the average dynamical effect of the bending modes neglected. It is found[24,25] that the lifetimes obtained with a RDQ model which incorporates the zero-point energy of the bending modes neglected (i.e., which considers the full-dimensional vdW energy), are higher than those calculated when the RDQ model does not incorporate that zero-point energy. This is why the present lifetimes and those of Ref. 25 are higher than the lifetimes obtained with the RDQ model of Le Quéré and Gray[23] (which also considers the three stretching modes of Cl_2-Ne_2, but it does not include the bending zero-point energy). This result is probably related to the energy-gap law.[36] Following this law, as the energy difference between the initial and final levels v and v_f of the BC diatomic matches the vdW energy of the $BC-Rg_2$ complex (i.e., the kinetic energy available for the Rg fragments $\epsilon\rightarrow 0$), the predissociation linewidth increases, and therefore the lifetime decreases. When the zero-point energy of the modes neglected is not included in the model, the vdW energy becomes lower (larger in absolute value) than the full one (see Table I), leading to smaller ϵ and thus to lower lifetimes. As discussed previously,[25] upon gradual inclusion of the couplings between the stretching and bending modes (potential acceptors of energy) in the model of Ref. 25, the lifetimes calculated are expected to decrease, converging towards the experimental result. Actually this behavior is found when comparing the present lifetimes to those of Ref. 25, as a result that the PS TDSCF approach incorporates partial coupling during the dynamics between the stretching (particularly the Cl_2 stretch vibration) and the bending modes.

The percentage of decrease of the present lifetimes with respect to those calculated with the RDQ model of Ref. 25 is listed in the last column of Table II. This variation gives a measure of the extent to which the PS TDSCF approach incorporates the stretching/bending couplings (and therefore how it improves the performance), with respect to the previous RDQ model. The convergence of the lifetimes ranges from about 11% to 17%. Interestingly, the percentage of convergence increases as v decreases, in parallel with the increasing intensity of the couplings between stretching and bending modes found in Ref. 25 and discussed below. Thus, the proposed PS TDSCF method is able to provide a larger correction as the couplings between the separated modes become increasingly stronger.

Good agreement (although still not completely quantitative) is found between the PS TDSCF and the experimental lifetimes in the range $v=10-13$. For $v=10-12$ the present lifetimes are closer to the experimental curve (see Fig. 1) than those calculated with the RDQ model of Le Quéré and Gray.[23] In particular, the PS TDSCF lifetime for $v=10$ is also closer to the experimental curve than the full-dimensional hybrid quantum-classical[21] prediction.

In the range $v<10$ the present lifetimes, although more converged than those of Ref. 25, still deviate largely from the experimental data and from the previous theoretical results of Refs. 21 and 23. It should be noted that the behavior of the lifetime with v predicted by the three quantum models shown in Fig. 1 deviates in a similar way from the experi-

TABLE II. Experimental and calculated decay lifetimes (in ps).

v	Experiment[a]	This work	RDQ1[b]	RDQ2[c]	Hybrid q/c[d]	Δ (%)
13	9.5	19.9	22.3	10.5	12.2	10.8
12		32.7		18.9	23.1	
11	44.4	53.4	60.0	29.7	41.2	11.0
10		87.0		50.1	55.6	
9		145.0	167.0	83.1	106.8	13.2
8	123.7	211.0	254.0	139.0	130.5	16.9
7		318.5	385.0	237.0		17.3

[a]Reference 6.
[b]Reference 25.
[c]Reference 23.
[d]Reference 21.

mental curve (nearly a straight line) as v decreases. This indicates that the increasing influence of the bending modes and their couplings to the other modes on the lifetime for low v levels of Cl_2-Ne_2, is important enough as to require a more explicit incorporation than that provided by the present and previous quantum models. Despite the failure for low v levels, the present PS TDSCF approach seems to perform well in order to predict the complex lifetime for $v \geqslant 10$ (at least in the range $v=10-13$ studied).

One of the strengths of the method proposed here is its computational efficiency. The extra computational effort required by the present calculations with respect to those of Ref. 25 [due to the time propagation of Eqs. (8)–(12)] is only 20%. It should be noted that most of this extra effort is translated into convergence of the calculated lifetimes (practically all the extra effort for $v=7$, 8, and more than half of it for higher v). The efficiency of the method lies on the fact that by representing the angular dependence of the Hamiltonian $\hat{H}$ in the basis functions of Eq. (16), all the quadratures over the angular modes are analytical. As a consequence, the calculation of time-dependent effective Hamiltonians and the time propagation of Eqs. (8) and (9) become very efficient. The efficiency in the treatment of the angular modes makes possible to apply the present method to a large variety of $BC-Rg_2$ systems, including those which would require a large number of angular basis functions. Application of the method to larger complexes, like $BC-Rg_3$, is also feasible. This would require to add an extra radial degree of freedom R_3, and to propagate a radial wave packet $\psi(r,R_1,R_2,R_3,t)$ (which would involve the main part of the computational effort). The additional angular modes θ_3 and ϕ_3 could be efficiently handled in the angular basis set representation.

TABLE III. Calculated and experimental Cl_2 fragment vibrational populations (in percentage) for the dissociation channels $v-1$, $v-2$, and $v-3$. Some small percentages of population found in Ref. 21 for the channels $v-4$ and $v-5$, are not listed.

	v	$v-1$	$v-2$	$v-3$
This	13	0.4	92.8	6.8
work	12	1.0	93.9	5.1
	11	5.2	91.2	3.6
	10	12.0	85.5	2.5
	9	22.0	76.3	1.7
	8	36.6	62.4	1.0
	7	53.3	46.2	0.5
RDQ1[a]	13	0.5	93.6	5.9
	11	13.4	83.4	3.2
	9	44.9	53.9	1.2
	8	59.6	39.7	0.6
	7	73.4	26.3	0.3
RDQ2[b]	13	1	94	5
	12	1	95	5
	11	1	96	4
	10	1	96	3
	9	2	96	2
	8	2	96	2
	7	3	96	1
Hybrid	13	1.3	73.7	18.4
q/c[c]	12	3.1	76.0	15.6
	11	7.9	75.4	13.8
	10	11.8	75.1	11.1
	9	17.1	74.6	7.0
	8	23.9	69.1	6.2
	7	25.6	68.5	5.4
Experiment[d]	9	19	81	
	7	79	21	

[a]Reference 25.
[b]Reference 23.
[c]Reference 21.
[d]Reference 6.

B. Vibrational distributions of Cl_2

Vibrational distributions of the $Cl_2(v_f)$ fragment ($v_f=v-1$, $v-2$, $v-3$) are calculated following the procedure described in Ref. 25. The present vibrational populations are collected in Table III along with the experimental and previously calculated ones. In the experiment the $v-3$ channel was weakly observed and no quantitative measurements of the populations were reported. In the case of the $v-1$ and $v-2$ populations, the experimental results for $v \geqslant 10$ (not shown in Table III) are that 100% of the population corresponds to the $v-2$ channel.

The present vibrational populations for the $v-3$ channel are very similar (only slightly higher) to those obtained with the two previous RDQ models.[23,25] The quantum-mechanical $v-3$ populations are low in general, in agreement with the experimental observation. The hybrid quantum-classical calculations of Bastida *et al.*[21] predict significantly higher $v-3$ populations. It has been discussed in Ref. 21 that a RDQ model which neglects the bending modes is expected to give lower populations for the channels $v-3$, $v-4$, ..., due to underestimating IVR effects. Actually, the present model, which incorporates a larger influence of the bending modes than that of Ref. 25, leads to slightly higher $v-3$ populations.

The populations associated with the $v-1$ and $v-2$ channels are remarkably different from those of Ref. 25. As discussed in Ref. 25, the $v-1$ populations calculated in that work were expected to be overestimated due to two factors. One factor was to neglect the dynamical effect of the energy-acceptor bending modes in the previous RDQ model. The other factor was related to the underestimate of the $v-2$ and $v-3$ populations due to absorption of $Cl_2-Ne+Ne$ wave packet components before total fragmentation into $Cl_2(v_f)+2Ne$ ($v_f=v-2$, $v-3$) is achieved. In the present treatment the negative effects of these two factors are diminished to a large extent. First, the effect of the bending modes is partially incorporated into the dynamics. Second, by increasing the grid size and placing the absorption region farther away in the asymptotic region, a larger amount of Cl_2-Ne wave packet components (which have a longer fragmentation time scale) are allowed to dissociate before they are absorbed.

The vibrational populations calculated with the PS TDSCF approach converge in the correct direction (with respect to those of Ref. 25), in the sense that they agree better with the experimental findings. Indeed, practically all the decrease of the $v-1$ population goes to the $v-2$ channel, while the $v-3$ populations remain low. For $v \geqslant 9$ the populations of the three channels $v-1$, $v-2$, and $v-3$ agree well with the

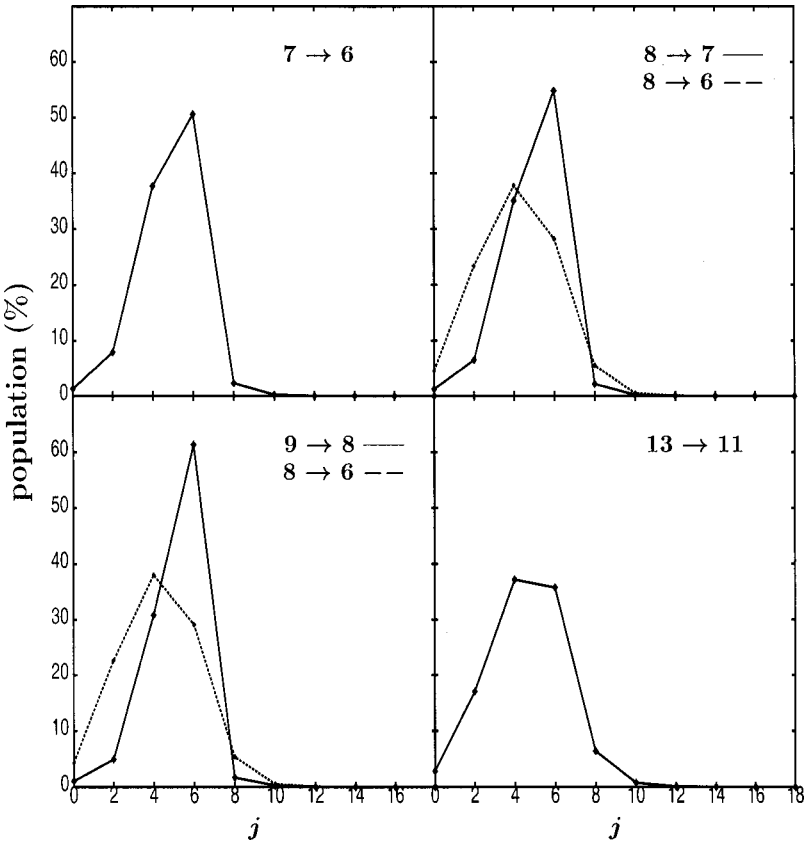

FIG. 2. Calculated Cl_2 fragment rotational state distributions for vibrational predissociation of Cl_2-Ne_2 through the vibrational channels $v_f=v-1$ and $v_f=v-2$. The initial v and final v_f vibrational states of Cl_2 are given by the lables $v\rightarrow v_f$ in each plot.

experimental results. This is consistent with the good agreement found between the PS TDSCF and the experimental lifetimes for high v levels, and confirms that the present method works well in that region of vibrational excitations.

For $v<9$ the agreement between the PS TDSCF and the experimental populations for the $v-1$ and $v-2$ channels is quantitatively worse. This is also consistent with the poorer performance of the method in the calculation of the lifetime as v decreases. However, the approach is able to predict the experimental finding that for $v=7$ there is a reversal of population and the $v-1$ channel becomes dominant. This result, already predicted by the RDQ model of Ref. 25, was not found in the simulations of Le Quéré and Gray[23] and Bastida *et al.*[21] (see Table III). Thus the PS TDSCF vibrational populations provide the best global agreement with the populations measured in the whole range $v=7-13$ of vibrational excitations studied.

A possible explanation of the fast increase of the $v-1$ population found experimentally for $v\leqslant 9$, could be related to the increasing intensity of the couplings between the bending and the stretching modes as v decreases. Once the $v-1$ channel is open, fragmentation of the two vdW bonds of the Cl_2-Ne_2 complex through this channel occurs when each vdW stretching mode gets a share of the vibrational quantum of energy enough to break it. Part of the vibrational energy is absorbed by the bending modes. Events in which direct energy transfer from Cl_2 places into the two vdW stretching modes an amount of energy similar and enough to dissociate them are rather unlikely. It is more likely that one stretching mode gets energy in excess, while the share of energy available for the other stretching mode is insufficient to break it. In principle this would lead to fragmentation of the second vdW bond through the $v-2$ (or $v-3$) channel. The situation may change if the couplings between the bending and the stretching modes are strong enough. Through those couplings the bending modes can channel part of the energy they have absorbed, and even part of the excess energy of one of the vdW stretching modes, towards the other stretching mode which got insufficient energy to break. Such an efficient energy transfer through the bending/stretching couplings would make more likely the $v-1$ channel, and would explain the high vibrational populations found experimentally for low v levels.

Evidence of increasingly strong bending/stretching couplings as v decreases, supporting the above possible mechanism, are found in Ref. 25 and in this work. In addition, the rotational distributions of the Cl_2 fragment esperimentally observed for the $v-1$ channel (see left panels of Fig. 7 in Ref. 21) also seem to support the above explanation. Such distributions cool down slightly as v decreases from $v=9$ to $v=7$, when the opposite behavior is expected since as v decreases E_v-E_{v-1} increases and there is more energy available for the rotational modes. This cooling could be an indication that part of the rotational energy is being channeled towards the stretching modes.

Aside from the level of accuracy in the description of the bending/stretching couplings, possible deficiencies in the potential surface used could be partially responsible for the disagreement (where found) between calculated (in the present and previous works) and observed magnitudes. With the present potential surface the vdW bond energies obtained variationally are about 125 cm^{-1} (see Table I), while the

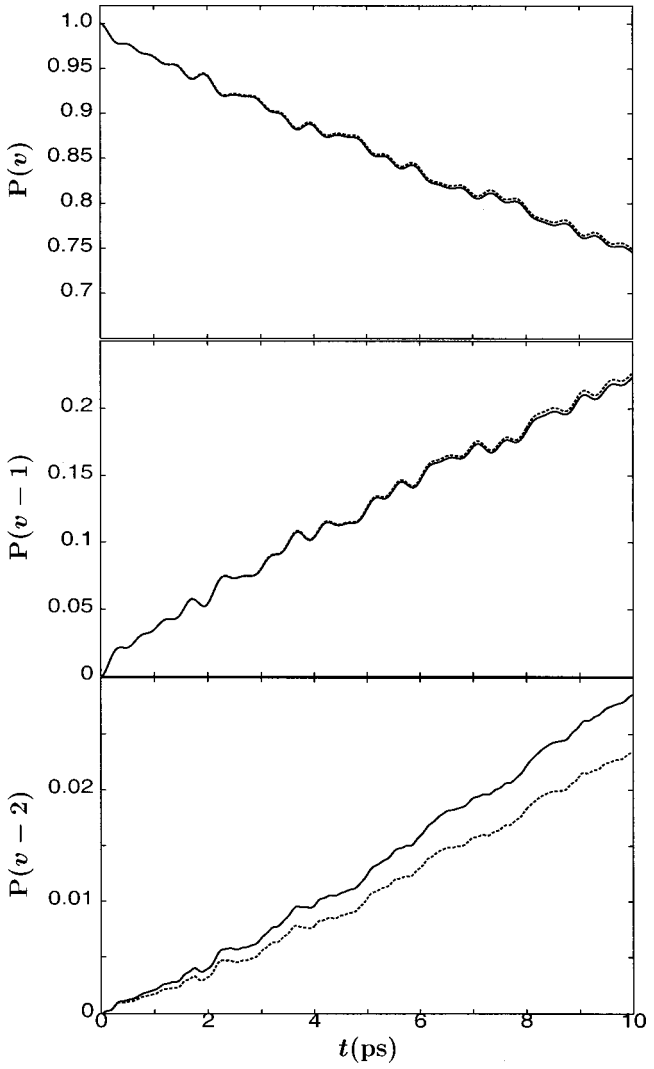

FIG. 3. Calculated time evolution of the populations in the vibrational states v (top panel), $v-1$ (middle panel), and $v-2$ (bottom panel) upon vibrational predissociation of $I_2(B, v=21)-Ne_2$. Two PS TDSCF calculations are shown including four (solid line) and three (dashed line) I_2 vibrational channels. See the text for details.

experimental vdW bond energy[6] was determined to be between 145.6 cm^{-1} and 148.6 cm^{-1} for $v=9$. There is a significant difference of more than 20 cm^{-1}. One of the consequences is that with the variational resonance energies the $v-1$ channel is closed only for $v=13$, while with the experimental vdW bond energy this channel is closed for $v \geqslant 10$, which is supported by the measured $v-1$ vibrational populations. This indicates that the Cl_2-Ne_2 potential surface of the B electronic state could need some refinement. Upon such a refinement, the present PS TDSCF method could provide a more quantitative description of both the lifetime and the vibrational distribution for $v \geqslant 9$, where the bending/stretching couplings are reasonably well described at the present level.

C. Rotational distributions of Cl_2

The explicit incorporation of the bending modes in the present PS TDSCF treatment allows one to calculate rotational distributions of the Cl_2 fragment. This makes a difference with previous RDQ models where only the stretching modes of the cluster are explicitly considered. Rotational distributions of the $Cl_2(v_f, j)$ fragment have been calculated for the channels $v_f=v-1$ and $v_f=v-2$ for the resonance states associated with $v=7-9,13$, and they are displayed in Fig. 2. To this purpose the asymptotic wave packet $\Psi^{\mathrm{TDSCF}}(r, R_1, R_2, \theta_1, \theta_2, \phi, t)$ is projected onto all the states of the fragments $Cl_2(v_f, j)+Ne+Ne$ accessible at the corresponding total energy of the complex. The projection is carried out in the asymptotic region 25.0 a.u. $\leqslant R_i \leqslant$ 57.0 a.u. $(i=1,2)$.

As discussed in Sec. II C, the partial, limited description of the bending/stretching couplings provided by the PS TDSCF method is expected to underestimate energy transfer towards the rotational modes, and therefore rotational excitation. Indeed this is the result found, and the rotational distributions of Fig. 2 are colder than the experimental ones (see Fig. 7 in Ref. 21). In the case of the $v_f=v-1$ channel for $v=7-9$, the PS TDSCF method is able to predict that the positions of the maxima of the rotational distributions occur at the same j level as that observed experimentally ($j=6$ for $v=8, 9$), or close to it (the experimental peak for $v=7$ is $j=4$, while the calculated one is $j=6$). Since the j distributions of the initial resonance states peak at $j=4$, the maxima found in the $v_f=v-1$ rotational distributions indicate that the method accounts for some energy transfer to the rotational modes. However, the PS TDSCF approach is not able to describe excitation to higher rotational levels, and the population of $j \geqslant 8$ is clearly underestimated. The failure of the method in reproducing the Cl_2 rotational distributions is more evident in the case of the very cold $v_f=v-2$ distributions of Fig. 2, as compared to the experimental ones. The result that the PS TDSCF method underestimates rotational excitation was already found in simulations of the VP dynamics of Cl_2-Ne.[37]

D. Application to VP of $I_2(B,\ v=21)-Ne_2$

In order to test further the present PS TDSCF approach, the VP dynamics of the $I_2(B, v=21)-Ne_2$ complex has been simulated to compare with the MCTDH results reported in Ref. 27. Assuming that the MCTDH calculations are practically converged, as shown by the convergence tests reported by Meier and Manthe,[27] the MCTDH results can be considered as exact ones. Comparison with such results provides a stringent test for the PS TDSCF method.

Using the same potential-energy surface[38] of Ref. 27 the initial resonance state of $I_2(B, v=21)-Ne_2$ is calculated variationally. Similarly as with Cl_2-Ne_2, in the variational calculation only one function is considered for the I_2 vibrational stretching mode (that corresponding to $v=21$). In practice this means that in the initial wave function the I_2 stretch and the vdW modes are factorized. A similar assumption was made in the relaxation method employed in Ref. 27, so the two calculations of the initial state should be very close. Indeed, the vdW binding energy obtained variationally is -143.4 cm^{-1}, very close to the energy of -144 cm^{-1} found by Meier and Manthe[27] with the relaxation method.

In the wave packet propagation the same radial grid and

absorption parameters as in Ref. 27 have been used. These parameters are $R_0=5.0$ a.u., $\Delta R=0.25$ a.u., and $N_R=192$ grid points, and $R_{abs}=20.0$ a.u. and $\alpha=0.028$ a.u.$^{-2}$ for the parameters of the absorption exponential functions. An expansion on 1800 angular basis functions $\eta_{l_1,l_2,L}(\theta_1,\theta_2,\phi)$ is used for the angular wave packet, with $l_1^{max}=l_2^{max}=28$ and $L^{max}=28$. Propagation of the radial and angular wave packets is carried out with time steps $\Delta t_1=0.01$ ps and $\Delta t_2=0.000\,625$ ps, respectively, up to a final time $t=10$ ps. This is the propagation time for which convergence tests have been reported for the MCTDH calculations.[27]

Two PS TDSCF calculations have been carried out, one including four terms $\nu=v$, $v-1$, $v-2$, $v-3$ in the expansion of Eq. (13), the other one including only three terms, $\nu=v$, $v-1$, $v-2$. The time evolution of the total populations in the vibrational states v, $v-1$, and $v-2$ [see Eq. (5) and Fig. 2 in Ref. 27] are the most converged quantities reported in the work of Meier and Manthe, and therefore they will be used to compare with the PS TDSCF results. The time evolution of these populations obtained with the two PS TDSCF calculations are shown in Fig. 3.

Very good agreement is found between the PS TDSCF and the MCTDH time evolutions, particularly for the v and $v-1$ populations. The undulations displayed by the PS TDSCF curves are originated in the factorization of the radial and angular modes in the initial state, as discussed elesewhere.[25] After 10 ps the two most converged MCTDH calculations, termed 20/6 and 20/5 in Ref. 27, yield populations of $\approx$77.5% and $\approx$76.0% in v, and $\approx$21.0% and $\approx$22.5% in $v-1$, respectively. After the same propagation time the PS TDSCF calculations considering four and three I_2 vibrational channels give populations of 74.6% and 74.9% in v, and 22.4% and 22.7% in $v-1$, repectively, very close to the MCTDH values. The good agreement between the PS TDSCF and MCTDH results for the decay curve $P(v)$ is particularly interesting, since the resonance decay lifetime can be extracted from that curve. The implication is that the PS TDSCF and MCTDH methods would lead to similar lifetimes.

For the $v-2$ populations, the 20/6 and 20/5 MCTDH calculations give $\approx$1.5% and $\approx$1.8%, respectively, after 10 ps. The corresponding PS TDSCF populations when four and three vibrational channels are considered are 2.8% and 2.3%, repectively, showing a somewhat lower level of agreement with the MCTDH results than in the case of the v and $v-1$ populations. This larger discrepancy is not surprising since, due to the small intensity of the $v-2$ wave packet component ($<3\%$), the uncertainties of both the PS TDSCF and the MCTDH methods in the calculation of this population are expected to be larger.

It is apparently surprising the result that the PS TDSCF calculation considering only three vibrational channels is slightly closer to the MCTDH results than the more converged PS TDSCF calculation which includes the additional $v-3$ channel. This result might just be a coincidence. Another possible explanation is that the five single-particle functions used in Ref. 27 to represent the I_2 stretch vibration might be insufficient to represent four vibrational channels (no convergence tests increasing the number of these functions were reported in Ref. 27), leading to an incomplete representation of the $v-3$ channel. In the PS TDSCF approach the four vibrational channels are fully represented in Eq. (13).

IV. CONCLUSIONS

A full-dimensional time-dependent quantum approach to simulate the vibrational predissociation dynamics of $BC-Rg_2$ systems has been proposed. The method applies the partially-separable time-dependent self-consistent-field approximation to express the total, six-dimensional wave function as a product of two functions, one including the three stretching modes of the system, the other one describing the three bending modes. Within each group the modes retain the full coupling. The equations of the method make possible partial interaction between the separated modes through mean-field Hamiltonians. The bending coordinates are represented in an angular basis set which, along with the mode separation assumed, makes the approach suggested very efficient.

The method is tested by simulating the vibrational predissociation dynamics of Cl_2-Ne_2 in the Cl_2 vibrational excitation range $v=7-13$, and comparing the results with experimental data and previous simulations. The present approach is found to involve only a 20% of extra computational effort with respect to a previous reduced-dimensional quantum model which considered only the three stretching modes of the system. This result assesses the efficiency of the method. Most of the extra effort is translated into convergence (towards the experimental values) of the currently calculated lifetimes and Cl_2 vibrational populations, as compared to those obtained with the previous reduced-dimensional model.

Good, nearly quantitative agreement with experiment (within the uncertainties of the potential surface used) is found for the resonance lifetimes and Cl_2 vibrational distributions calculated for the higher Cl_2 vibrational excitations in the range studied. For $v\leqslant 9$ the calculated lifetimes exhibit large deviations from the experimental results, showing a similar behavior with decreasing v to the lifetimes obtained with earlier reduced-dimensional quantum models. Such a behavior is attributed to an increasingly important dynamical role of the bending modes and their couplings to the stretching modes as v decreases. The calculated Cl_2 fragment vibrational populations for $v<9$ agree worse with the experimental measurements, consistently with the poorer performance of the method as the intensity of the bending/stretching couplings increases. The approach is still able to predict the experimental finding that the population of the $v-1$ channel increases rapidly as v decreases from $v=9$, and becomes dominant for $v=7$. This result was unpredicted in previous reduced-dimensional quantum and full-dimensional hybrid quantum-classical simulations. The present method fails in reproducing the experimental Cl_2 rotational distributions, underestimating rotational excitation of the Cl_2 fragment. This failure is mainly due to the decoupling between the bending modes and the Cl_2 stretching vibration where the energy is initially deposited.

The PS TDSCF approach is also tested against MCTDH calculations by simulating the VP dynamics of $I_2(B,v=21)-Ne_2$ and comparing the time evolution of the vibrational populations. An encouragingly good agreement is found between the PS TDSCF simulation and the two most converged MCTDH calculations, which assesses the reliability of the PS TDSCF method. Related to this agreement is probably the fact that the influence of the angular modes in the dynamics of $I_2(B,v=21)-Ne_2$ is not very strong. In addition, the $I_2(B,v=21)-Ne_2$ simulation demonstrates that the PS TDSCF method can handle efficiently large expansions for the angular wave packet representation (with 1800 angular basis functions in this case).

The approach suggested in this work appears as an efficient tool to describe the main dynamical features of the vibrational predissociation of $BC-Rg_2$ clusters. The method seems to provide reliable predictions (at a semiquantitative or even nearly quantitative level) of most of the observable magnitudes of interest, as long as the couplings between the separated modes are not strong [which is the case of Cl_2-Ne_2 for $v=9-13$ and $I_2(B,v=21)-Ne_2$]. When such couplings become more relevant the level of accuracy achieved by this model is only qualitative. The efficiency of the approach makes feasible its application to larger clusters.

ACKNOWLEDGMENTS

This work was supported by C.I.C.Y.T., Spain, Grant No. BCM-2001-2179, and by the EU network TMR Grant No. HPRN-CT-1999-00005.

[1] W. Sharfin, K.E. Johnson, L. Warton, and D.H. Levy, J. Chem. Phys. **71**, 1292 (1979).
[2] J.E. Kenny, K.E. Johnson, W. Sharfin, and D.H. Levy, J. Chem. Phys. **72**, 1109 (1980).
[3] A. Burroughs, G. Kerenskaya, and M.C. Heaven, J. Chem. Phys. **115**, 784 (2001).
[4] B.A. Swartz, D.E. Brinza, C.M. Western, and K.C. Janda, J. Phys. Chem. **88**, 6272 (1984).
[5] J.C. Drobits and M.I. Lester, J. Chem. Phys. **86**, 1662 (1987).
[6] S.R. Hair, J.I. Cline, C.R. Bieler, and K.C. Janda, J. Chem. Phys. **90**, 2935 (1989).
[7] D.D. Evard, C.R. Bieler, J.I. Cline, N. Sivakumar, and K.C. Janda, J. Chem. Phys. **89**, 2829 (1988); C.R. Bieler, D.D. Evard, and K.C. Janda, J. Phys. Chem. **94**, 7452 (1990).
[8] W.D. Sands, C.R. Bieler, and K.C. Janda, J. Chem. Phys. **95**, 729 (1991).
[9] D.M. Willberg, M. Gutmann, J.J. Breen, and A.H. Zewail, J. Chem. Phys. **96**, 198 (1992); M. Gutmann, D.M. Willberg, and A.H. Zewail, *ibid.*, **97**, 8037 (1992); **97**, 8048 (1992).
[10] N. Halberstadt, J.A. Beswick, and K.C. Janda, J. Chem. Phys. **87**, 3966 (1987).
[11] J.I. Cline, N. Sivakumar, D.D. Evard, C.R. Bieler, B.P. Reid, N. Halberstadt, S.R. Hair, and K.C. Janda, J. Chem. Phys. **90**, 2605 (1989).
[12] O. Roncero, J.A. Beswick, N. Halberstadt, P. Villarreal, and G. Delgado-Barrio, J. Chem. Phys. **92**, 3348 (1990).
[13] S.K. Gray and C.E. Wozny, J. Chem. Phys. **94**, 2817 (1991).
[14] A. Rohrbacher, T. Ruchti, K.C. Janda, A.A. Buchachenko, M.I. Hernández, T. González-Lezana, P. Villarreal, and G. Delgado-Barrio, J. Chem. Phys. **110**, 256 (1999).
[15] A. García-Vela, P. Villarreal, and G. Delgado-Barrio, J. Chem. Phys. **92**, 6504 (1990).
[16] A. García-Vela, P. Villarreal, and G. Delgado-Barrio, J. Chem. Phys. **94**, 7868 (1991).
[17] J. Rubayo-Soneira, A. García-Vela, P. Villarreal, and G. Delgado-Barrio, Chem. Phys. Lett. **243**, 236 (1995); A. García-Vela, J. Rubayo-Soneira, G. Delgado-Barrio, and P. Villarreal, J. Chem. Phys. **104**, 8405 (1996).
[18] Z. Li, A. Borrmann, and C.C. Martens, J. Chem. Phys. **97**, 7234 (1992).
[19] M.I. Hernández, A. García-Vela, C. García-Rizo, N. Halberstadt, P. Villarreal, and G. Delgado-Barrio, J. Chem. Phys. **108**, 1989 (1998).
[20] S. Fernández Alberti, N. Halberstadt, J.A. Beswick, A. Bastida, J. Zúñiga, and A. Requena, J. Chem. Phys. **111**, 239 (1999).
[21] A. Bastida, B. Miguel, J. Zúñiga, A. Requena, N. Halberstadt, and K.C. Janda, J. Chem. Phys. **111**, 4577 (1999).
[22] P. Villarreal, A. Varadé, and G. Delgado-Barrio, J. Chem. Phys. **90**, 2684 (1989).
[23] F. Le Quéré and S.K. Gray, J. Chem. Phys. **98**, 5396 (1993).
[24] J. Campos-Martínez, M.I. Hernández, O. Roncero, P. Villarreal, and G. Delgado-Barrio, Chem. Phys. Lett. **246**, 197 (1995).
[25] M. Ceotto and A. García-Vela, J. Chem. Phys. **115**, 2146 (2001).
[26] O. Roncero, G. Delgado-Barrio, M.I. Hernández, J. Campos-Martínez, and P. Villarreal, Chem. Phys. Lett. **246**, 187 (1995).
[27] C. Meier and U. Manthe, J. Chem. Phys. **115**, 5477 (2001).
[28] A. García-Vela, J. Chem. Phys. **111**, 8286 (1999).
[29] P. Villarreal, O. Roncero, and G. Delgado-Barrio, J. Chem. Phys. **101**, 2217 (1994).
[30] R.B. Gerber and M.A. Ratner, Adv. Chem. Phys. **70**, 97 (1988).
[31] R.D. Coalson, Chem. Phys. Lett. **165**, 443 (1990).
[32] R.N. Zare, *Angular Momentum* (Wiley, New York, 1988).
[33] A.R. Edmonds, *Angular Momentum in Quantum Mechanics* (Princeton University Press, Princeton, 1957).
[34] H. Tal-Ezer and R. Kosloff, J. Chem. Phys. **81**, 3967 (1984).
[35] V. Engel, Chem. Phys. Lett. **189**, 76 (1992).
[36] J.A. Beswick and J. Jortner, Adv. Chem. Phys. **47**, Part I, 363 (1981).
[37] A. García-Vela, Chem. Phys. Lett. **290**, 155 (1998).
[38] In Table I of Ref. 27 the values of the Morse parameters x_0 and α have been exchanged. They should read $x_0=8.24$ a.u. and $\alpha=0.83$ a.u.$^{-1}$ for the I–Ne interaction, and $x_0=5.84$ a.u. and $\alpha=1.10$ a.u.$^{-1}$ for the Ne–Ne interaction.